



Design and Vibration Control Optimization of an Aluminum Alloy Deck System for a Pedestrian Cableway Bridge

Tianhu Jing^a, Yu Yan*

Guangxi Key Laboratory of Green Building Materials and Construction Industrialization, Guilin University of Technology, Guilin, 541004, China

^a 908801689@qq.com, tel:19126047867; * 1519898546@qq.com

Abstract. To meet the stringent requirements of lightweight and durability in pedestrian aerial ropeway bridges, this study proposes a novel aluminum alloy deck system and conducts a comprehensive dynamic performance analysis using ANSYS finite element software. By comparing the dynamic characteristics of the proposed system with those of a conventional steel-wood composite deck, the vibration response and walking comfort under pedestrian-induced excitations are systematically evaluated. The results indicate that, relative to traditional systems, the aluminum alloy deck significantly enhances the global stiffness and fundamental frequency of the structure, demonstrating superior vibration control capabilities. However, certain deficiencies remain in terms of pedestrian comfort and vibration mitigation performance, necessitating further optimization. To address these issues, tuned mass dampers (TMDs) are introduced as an effective vibration control strategy. Various TMD configurations are designed and assessed with respect to their efficiency in reducing both lateral and vertical vibrations, as well as their practical feasibility in construction. Finite element modeling is employed to evaluate the damping effectiveness of each scheme. Findings reveal that symmetrically arranged lateral TMDs can effectively suppress lateral vibrations, while placing TMDs at locations with peak vertical displacements significantly improves vertical vibration reduction. The optimized TMD layout not only ensures constructability but also substantially enhances the overall dynamic performance and walking comfort of the aluminum alloy deck system. This study confirms the feasibility and superiority of aluminum alloy deck systems in lightweight, durable bridge applications and offers a practical and theoretical framework for pedestrian-induced vibration control in ropeway bridge engineering.

Keywords: Pedestrian cableway bridge, Aluminum alloy deck system, Tuned Mass Damper.

1 Introduction

The Pedestrian suspension bridges have seen widespread application in scenic areas in recent years due to their lightweight structure, ease of construction, cost-effectiveness,

© The Author(s) 2025

G. Zhao et al. (eds.), *Proceedings of the 2025 8th International Conference on Traffic Transportation and Civil Architecture (ICTTCA 2025)*, Atlantis Highlights in Engineering 39,

https://doi.org/10.2991/978-94-6463-793-9_63

and strong adaptability to natural landscapes. However, conventional bridge deck systems—typically composed of timber or steel-timber composites—are prone to corrosion and aging in outdoor environments, resulting in limited service life and increased maintenance costs. These durability issues have significantly hindered the long-term promotion and application of this bridge type. To enhance the long-term performance of pedestrian suspension bridges, the development of new deck materials featuring lightweight, high strength, corrosion resistance, and environmental sustainability has become a key research focus. Aluminum alloys, characterized by high specific strength, excellent corrosion resistance, good formability, and recyclability, have demonstrated remarkable advantages in fields such as marine engineering, naval architecture, transportation, and selected bridge structures. Their intrinsic properties align particularly well with the lightweight design demands of pedestrian suspension bridges. Therefore, integrating aluminum alloys into the deck system holds significant engineering and academic value in terms of extending service life, improving environmental adaptability, and reducing life-cycle maintenance costs ^[1,2].

Existing studies ^[3] have demonstrated that the overall mass and stiffness of pedestrian bridges are closely related to their dynamic characteristics. When bridge materials exhibit low density and low elastic modulus, the resulting structural damping tends to decrease, increasing the likelihood that the bridge's natural frequency will approach typical pedestrian walking frequencies. Under such conditions, pedestrian-induced excitations can lead to significant vibrations or even human–structure resonance, which poses serious concerns for pedestrian comfort and structural dynamic safety. Tuned Mass Dampers (TMDs), which mitigate vibrations by generating inertial forces in the opposite direction through frequency-tuned auxiliary masses, have been widely recognized as an effective method for suppressing pedestrian-induced vibrations. However, most existing research has focused on deck systems composed of steel or steel-timber composites. For pedestrian suspension bridges—structures that typically lack longitudinal deck girders and possess relatively low overall stiffness—studies on the integration of aluminum alloy deck systems in combination with suitable damping solutions remain sparse. In particular, there is a clear lack of detailed dynamic response evaluations under crowd-induced loads for long-span suspension bridges utilizing aluminum decks, as well as a shortage of targeted optimization strategies for vibration mitigation. In other words, current research is insufficient to fully support the large-scale application of such innovative deck systems in practical pedestrian suspension bridge projects ^[4,5].

To address the aforementioned challenges, finite element (FE) analysis offers a powerful tool to accurately simulate and evaluate bridge vibration behavior and pedestrian comfort levels under various influences, including structural self-weight, human-induced loads, and vibration control devices. By establishing a comprehensive FE model of a pedestrian suspension bridge featuring an aluminum alloy deck, the dynamic performance differences between aluminum and conventional steel-timber deck systems can be systematically assessed. Furthermore, the effectiveness of different TMD configurations—considering various placement schemes and parameter settings—can be quantitatively evaluated. Integrating these analytical outcomes with practical considerations such as constructability and maintenance requirements enables the development

of optimized, feasible design solutions for aluminum alloy pedestrian suspension bridges. This simulation-driven research framework not only provides a scientific basis for improving the comfort and safety performance of innovative deck systems, but also lays a solid foundation for future engineering applications and theoretical advancements in this field [6,7].

2 Project Overview

2.1 Background Bridge

A single-span pedestrian cableway bridge located in a scenic area features a main cable with a calculated span of 147.652 meters and a designed sag of 3.5 meters under the full dead load condition, corresponding to a sag-to-span ratio of 1/42.2. The main cable is anchored at both ends using rock-anchored anchorages, with a clear distance between abutments of 141.2 meters and a net pedestrian walkway width of 2.02 meters. The bridge adopts eight PES(C)5-109 parallel steel wire strands as main cables, each composed of epoxy-coated steel wires with dual-layer HDPE sheathing and a specified tensile strength of 1670 MPa. The outer HDPE surface is further protected by a colored polyurea coating specifically designed for cable-supported bridges. The transverse arrangement of the main cables across the bridge deck follows a spacing pattern of $(33 + 5 \times 34.8 + 33)$ cm. The deck utilizes HM 200 \times 150 H-shaped steel beams as transverse floor beams, spaced longitudinally at 3-meter intervals. Deck paving consists of hardwood planks measuring 200 cm (transverse width) \times 29 cm (longitudinal length) \times 4 cm (thickness), with a 1 cm gap between adjacent planks, each reinforced with a 3 mm thick galvanized steel plate at the bottom. To enhance aerodynamic stability, inclined wind-resistant cable nets are symmetrically installed on both sides of the deck at an angle of 40° to the horizontal. The main wind-resistant cables span 126 meters with a 13.5-meter sag (sag-to-span ratio of 1/9.3), and both main and secondary cables are made of galvanized steel wire ropes with specifications of $\phi 40$ (6 \times 37S + IWR) and $\phi 16$ (6 \times 19S + IWR), respectively. According to design specifications, a crowd load of 3 kN/m² is considered for structural design, while operational pedestrian density is limited to 1.5 persons/m². During construction, in the first-phase dead load condition—after installation of the main cables and deck but prior to wind cable tensioning—a 30 cm upward pre-camber is introduced at mid-span of the main cable. Upon completion and tensioning of the wind-resistant cables (second-phase dead load condition), the deck reaches its design elevation under full dead load. This pre-camber effectively embeds the geometric stiffness induced by initial deformation into the completed structure, enhancing the post-construction global stiffness and dynamic performance of the bridge. The layout of the pedestrian cableway bridge in the scenic area is illustrated schematically in Figure 1.

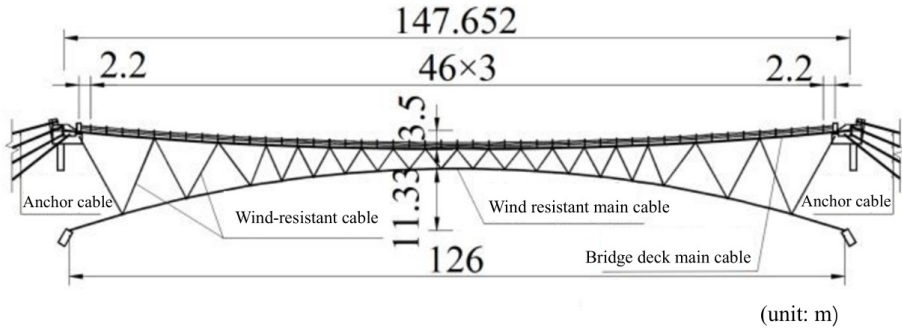


Fig. 1. Background bridge facade layout.

2.2 Aluminum Alloy Bridge Deck System Full Cycle Comparison

In the value-oriented engineering analysis of the pedestrian cableway bridge deck system, a "Life-Cycle Cost Radar Chart for Aluminum Alloy Decking" (See Figure 2) was developed to visualize and compare the comprehensive performance of aluminum alloy decks and conventional steel-timber decks across six key dimensions: construction cost, maintenance frequency, service life, residual/recycling value, structural weight, and construction period. Although aluminum alloy entails a relatively higher initial investment, its long-term economic advantages become evident through significantly reduced maintenance demands compared to the frequent anti-corrosion treatments and component replacements required by steel-timber systems. In terms of service life, the aluminum deck system, benefiting from superior corrosion resistance and fatigue performance, can achieve a service span exceeding 40 years—far surpassing that of typical steel-timber structures. From a sustainability perspective, aluminum alloy exhibits high recyclability and retains substantial residual value upon decommissioning, contributing to environmentally friendly, circular material utilization. Structurally, with a density only one-third that of steel, aluminum significantly reduces the dead load of the deck system, enabling overall superstructure light-weighting and substructure optimization. Additionally, the high degree of prefabrication and efficient connection techniques of aluminum components facilitate rapid on-site assembly and shortened construction duration. This radar-based multidimensional visualization enables a comprehensive, quantitative assessment of the aluminum alloy deck's life-cycle advantages, providing a clear and evidence-based foundation for its promotion and broader application in pedestrian cableway bridge projects^[8].

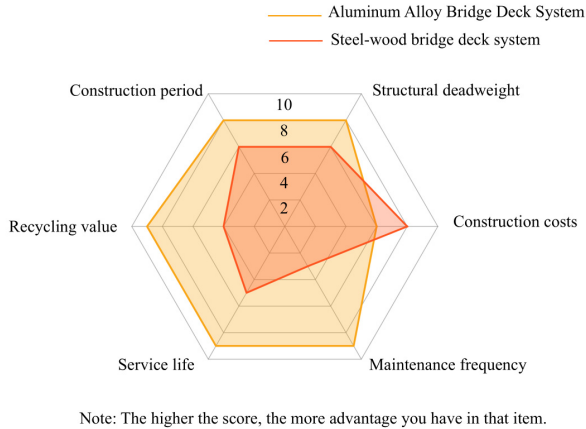


Fig. 2. Radar chart of the life cycle value of aluminum alloy and steel-wood bridge deck systems based on multi-dimensional performance indicators.

2.3 Aluminum Alloy Bridge Deck Design

Following the principle of functional and dynamic comparability with the reference pedestrian cableway bridge, the components of the preliminary bridge design were developed accordingly. The design process began with the specification of the main cables and their anchorage system. In the reference bridge, the characteristic value of the dead load per linear meter of the deck system—excluding the main cables—is approximately equal to that of the fully loaded pedestrian live load condition, indicating that the pedestrian load governs the cross-sectional design of the cable components. Therefore, the preliminary design adopts the same number, material, specifications, spatial arrangement, and final cable profile for the main load-carrying cables and wind-resistant cables as those in the reference bridge, while rock-anchored prestressed cable anchorages are retained for anchoring. Subsequently, the bridge deck system, including the aluminum alloy deck panels and stabilizing transverse beams, was designed using an engineering analogy approach. The 6061-T6 aluminum alloy, one of the most widely used materials in structural engineering, has a nominal yield strength comparable to Q235 steel. In the proposed bridge, the support spacing for the deck panels and transverse beams suspended from the main cables is approximately 1/2.27 and 1/2.58, respectively, of that used in the Tianjin Haihe Bengbu Bridge, which also features an aluminum alloy deck. Moreover, the deck width of the proposed pedestrian bridge is narrower than that of a typical single-lane highway bridge, resulting in lower load-bearing and stiffness demands on transverse members. Drawing from the detailing of the Haihe Bengbu Bridge, the proposed design specifies a cross-section for the 6061-T6 aluminum alloy deck panels with a transverse length of 2 meters (See Figure 3). At the same time, steel components in the reference bridge, such as stabilizing transverse beams and fasteners, are replaced with 6061-T6 aluminum alloy without altering their structural form or dimensions. This results in a complete aluminum alloy deck system

for the preliminary design. The overall unit mass per meter of the deck system, including the main cables, is approximately 63% that of the reference bridge, while the construction process and functional performance remain entirely consistent with the original design [9].

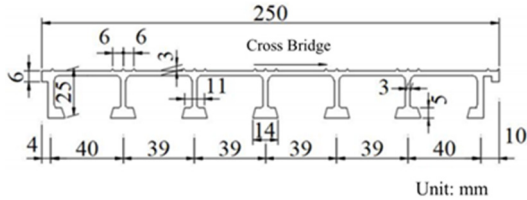


Fig. 3. Cross section of aluminum alloy bridge deck.

2.4 Creating an Analytical Model

In this study, the finite element modeling of the completed bridge under dead load conditions was conducted in two distinct phases to ensure precision and structural fidelity. For the first-phase dead load configuration, the shape-finding analysis of the main cable was based on the theoretical approach introduced in the previous chapter. A MATLAB-based program was developed, taking the floor beam locations as segmentation points of the main cable, with a designed mid-span sag of 3.5 m (including a 0.3 m pre-camber). Through iterative computation under self-weight, the planar configuration of the main cable and the initial strain in each cable segment were determined. Using the computed planar coordinates, a three-dimensional finite element model was subsequently constructed in ANSYS. The main cable was modeled using LINK10 elements, with initial strain parameters directly imported from the planar analysis. The deck panels and stabilizing transverse beams were modeled using BEAM4 elements, segmented at structural intersection points. The stiffness properties of the deck panels were calculated as the equivalent axial and flexural rigidity of the composite timber panel and underlying steel plate, while the remaining structural elements were assigned stiffness based on actual material and geometric characteristics. To ensure mass consistency with the planar model, the spatial model was calibrated so that the total mass per meter in the longitudinal direction remained identical. Fixed boundary conditions were applied at the ends of the main cable, and coupling constraints were imposed at the junctions between cable and deck elements. A static analysis incorporating the nonlinear behavior of the cable elements was performed in ANSYS under dead load. Validation results indicated that all nodal displacements were less than 1 mm, the relative deviations in horizontal and vertical reactions at the cable ends compared to the planar model were only 0.15% and 0.23%, respectively, and the total mass remained consistent between models, thereby confirming the accuracy of the spatial model. In the second-phase dead load configuration, the initial spatial model was extended by incorporating wind-resistant cables and wind-resistant main cables, modeled with LINK10 elements. These elements were arranged according to the design node coordinates, and their initial strain values were set based on 25% of their ultimate tensile capacity. A static analysis was

conducted to assess whether the vertical displacement at mid-span counteracted the 0.3 m pre-camber. If not satisfied, the strain parameters were iteratively adjusted and re-analyzed until convergence. The UPGEOM command was then used to update the model geometry by superimposing the verified nodal displacements onto the original coordinates, while replacing the strain parameters of the cable elements with the newly computed values. A final round of model validation, following the procedure used in the first phase, confirmed that all nodal displacements remained below 1 mm and the mid-span sag matched the target value of 3.5 m. The resulting second-phase spatial finite element model, comprising 8,224 nodes, 3,720 beam elements, and 4,036 cable elements, is illustrated in Figure 4.

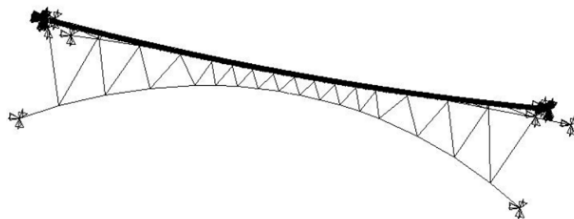


Fig. 4. Finite element analysis model of pedestrian cableway bridge.

3 Bridge Dynamic Characteristics Analysis

3.1 Natural Vibration Analysis of Two Pedestrian Cableway Bridges with Different Deck Systems Reating

According to the newly issued Chinese design code for pedestrian bridges, the completed structure must exhibit fundamental frequencies not lower than 3 Hz in the vertical direction and 1.2 Hz in the lateral direction. Should any structural modal frequency fall within the pedestrian-induced vibration sensitive ranges—1.25 to 3 Hz for vertical modes and 0.5 to 1.2 Hz for lateral modes—a further assessment of pedestrian comfort under the corresponding modes is required. For bridges with relatively lightweight superstructures and a significant proportion of pedestrian live load, it is essential to account for the dynamic mass contribution of pedestrians in the natural frequency analysis. The code recommends considering one-third of the pedestrian load as an equivalent participating mass. In this study, a finite element model representing the structure under the full dead load condition at Stage II completion is adopted. Using ANSYS software, eigenvalue modal analyses considering geometric nonlinearity are conducted under two scenarios: Case I, excluding the one-third pedestrian mass, and Case II, including it. The first 40 mode shapes are extracted for each scenario, with particular attention given to the fundamental frequency and those modes with frequencies below 3 Hz that fall within the sensitive range and are dominated by deck-level components. The

corresponding analysis results are summarized in Tables 1 and 2, with representative modal frequencies selected for detailed discussion^[10].

Table 1. Natural frequency of cableway bridge in modal condition 1/Hz.

Order	Steel and wood bridge deck system	Mode shape characteristics	Order	Aluminum bridge deck system	Mode shape characteristics
1	0.495	Symmetric lateral mode	1	0.566	Symmetric Lateral Mode
3	0.711	Antisymmetric lateral mode	2	0.753	Antisymmetric Lateral Mode
8	1.061	Symmetric lateral mode	9	1.127	Symmetric Lateral Mode
15	1.435	Antisymmetric vertical mode	15	1.53	Antisymmetric Vertical Mode
20	1.769	Symmetric vertical mode	20	1.879	Symmetric Vertical Mode
24	2.14	Antisymmetric vertical mode	25	2.279	Antisymmetric Vertical Mode
28	2.479	Symmetric vertical mode	30	2.632	Symmetric Vertical Mode
33	2.857	Antisymmetric vertical mode	35	3.045	Antisymmetric Vertical Mode

Note: The 35th mode frequency is greater than 3 Hz and is listed here for the convenience of discussion.

Table 2. Natural frequency of cable bridge in modal condition 2/Hz.

Order	Steel and wood bridge deck system	Mode shape characteristics	Order	Aluminum bridge deck system	Mode shape characteristics
1	0.462	Symmetric Lateral Mode	1	0.509	Symmetric Lateral Vibration
3	0.674	Antisymmetric Lateral Mode	2	0.695	Antisymmetric Lateral Vibration
8	1.006	Symmetric Lateral Mode	9	1.039	Symmetric Lateral Vibration
15	1.36	Antisymmetric Vertical Mode	15	1.409	Antisymmetric Vertical Vibration
19	1.679	Symmetric Vertical Mode	20	1.734	Symmetric Vertical Vibration
24	2.03	Antisymmetric Vertical Mode	25	2.101	Antisymmetric Vertical Vibration
26	2.352	Symmetric Vertical Mode	30	2.429	Symmetric Vertical Vibration

31	2.709	Antisymmetric Vertical Mode	35	2.807	Antisymmetric Vertical Vibration
----	-------	-----------------------------	----	-------	----------------------------------

3.2 Natural Vibration Analysis of Two Pedestrian Cableway Bridges with Different Deck Systems Reating

Substituting the structural fundamental frequency data of modal condition 2 of this project into the pedestrian comfort evaluation formula of the new Chinese pedestrian bridge standard, the evaluation criteria shown in Table 3 are obtained.

Table 3. Pedestrian comfort evaluation standards.

Comfort Level Classification	Comfort Evaluation	Reference Bridge		Pre-engineered bridges	
		Vertical peak acceleration limit (m/s ²)	Vertical peak acceleration limit (m/s ²)	Vertical peak acceleration limit (m/s ²)	Lateral peak acceleration limit (m/s ²)
CL1	optimal	[0,0.137]	[0,0.1]	[0,0.148]	[0,0.1]
CL2	Pass	[0.137,0.340]	[0.1,0.102]	[0.148,0.357]	[0.1,0.107]
CL3	Fail	[0.340,+∞]	[0.102,+∞]	[0.357,+∞]	[0.107,+∞]

4 Optimization of Tuned Mass Damper for Vibration Control

4.1 Vibration Mitigation Mechanism in Undamped Structures

Tuned Mass Damper (TMD) system, as a widely adopted vibration mitigation technique in structural engineering, is becoming increasingly prevalent in pedestrian suspension bridges. This system primarily consists of a mass block, a stiffness spring, and a damper. Its fundamental working principle lies in adjusting or counteracting the vibrations of the main structure through the motion of the attached mass. By properly tuning the natural frequency of the TMD to closely match a specific modal frequency of the main structure, the system can generate an inertial force in the opposite direction of the structural motion during vibration. This counteracting force effectively suppresses the dynamic response of the structure, thereby enhancing the bridge's dynamic performance and improving pedestrian comfort^[11,12].

$$\alpha_{\text{opt}} = 1 / 1 + \mu \quad (1)$$

$$\xi_{\text{opt}} = \sqrt{3\mu / 8(1 + \mu)} \quad (2)$$

$$k_{\text{opt}} = \alpha_{\text{opt}}^2 \omega_s^2 M_d \quad (3)$$

$$c_{\text{opt}} = 2\gamma_{\text{opt}} \alpha_{\text{opt}} \omega_s M_d \quad (4)$$

To address the comfort optimization problem of pedestrian suspension bridges, a TMD parameter optimization method based on an undamped structural model is adopted. Aiming to enhance pedestrian comfort, the optimal parameters of the TMD system are determined. The optimal stiffness and damping ratio are calculated based on the mass ratio between the total mass of the TMD and the modal participating mass of the bridge. According to the results of modal analysis, the 8th and 9th modes of the pre-designed bridge with an aluminum alloy deck system are considered. Among them, the 9th mode is selected as the control mode due to its maximum modal participating mass of 40,308.45 kg. Based on the analytical formulas presented in the previous section, the TMD system is designed accordingly. The total mass of the TMD is set to 5% of the modal participating mass, following the widely accepted theoretical recommendation, which is commonly applied to general structures such as buildings and bridges. The mechanical parameters of the TMD system are presented in Table 4^[13-15].

Table 4. TMD mechanical parameters.

Types of Tuned Mass Dampers	Single-Mass (kg)	Damping Ratio C_{opt} (N.S/m)	Stiffness Coefficient K_{opt} (N/m)
A	1007.71	1388	26765
B	671.81	925	17843
C	503.85	694	13382
D	335.90	463	8922

4.2 TMD Layout Scheme

To evaluate the vibration control performance of different TMD layout schemes, three critical cross-sections located at 1/4, 1/2, and 3/4 of the bridge span are selected for analysis. During the time-history analysis of structural acceleration response, all parameter settings are kept constant while the TMDs are arranged according to each layout scheme. Finite element models are established accordingly, and pedestrian harmonic loads are applied for dynamic simulation. The maximum vertical and lateral acceleration responses of the bridge are recorded to assess the effectiveness of each TMD configuration.

Scheme I: Two Type-A TMDs are adopted and arranged at the 1/4-span and 3/4-span cross-sections, respectively. After implementing the TMDs according to Scheme I, the bridge's acceleration responses under pedestrian loading in different directions are illustrated in Figure 5. Figures 6 and 7 compare the time-history curves of vertical and lateral acceleration responses at the 1/4-span cross-section, with and without TMDs under pedestrian excitation.

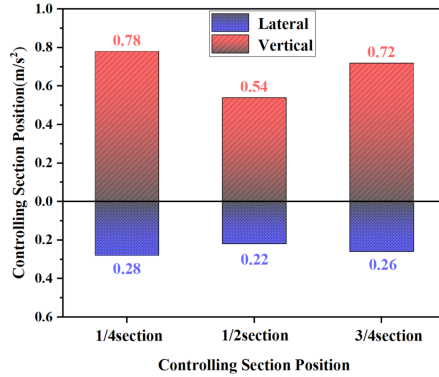


Fig. 5. Maximum acceleration response of each section based on Scheme I.

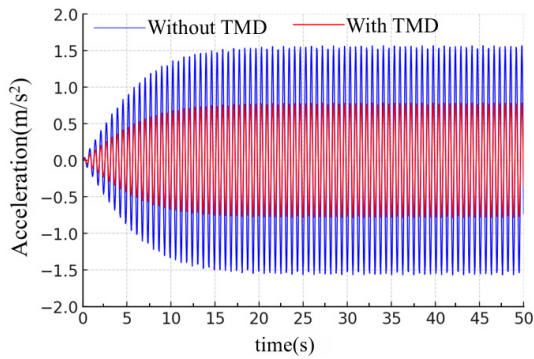


Fig. 6. Vertical acceleration comparison chart of scheme I.

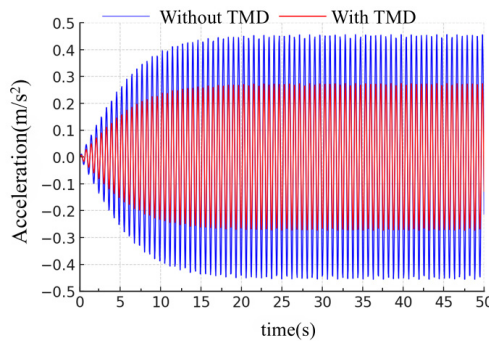


Fig. 7. Comparison of lateral acceleration of Scheme I.

Scheme II: Three Type-B TMDs are adopted and arranged at the 1/4-span, 1/2-span, and 3/4-span cross-sections, respectively. The acceleration responses of the pedestrian

suspension bridge under pedestrian loading in different directions are shown in Figure 8. Figures 9 and 10 compare the time-history curves of vertical and lateral acceleration responses at the 1/2-span cross-section, with and without TMDs under pedestrian excitation.

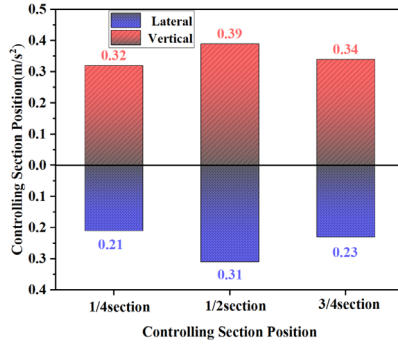


Fig. 8. Maximum acceleration response of each section based on Scheme II.

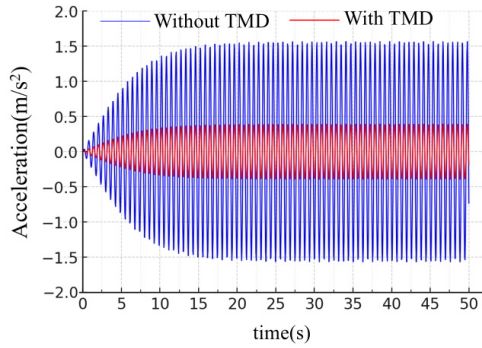


Fig. 9. Comparison of vertical acceleration of Scheme II.

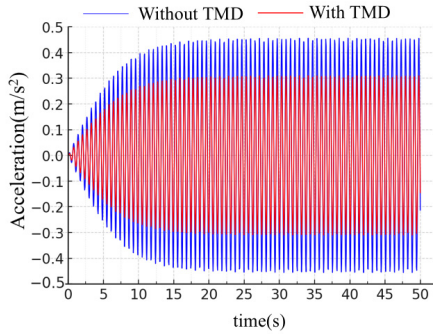


Fig. 10. Comparison of lateral acceleration of Scheme II.

Scheme III: Four Type-C TMDs are adopted, with two symmetrically arranged about the midpoint of the 1/4-span cross-section and the other two symmetrically arranged about the midpoint of the 3/4-span cross-section. The acceleration responses of the pedestrian suspension bridge under pedestrian loading in different directions are illustrated in Figure 11. Figures 12 and 13 compare the time-history curves of vertical and lateral acceleration responses at the 3/4-span cross-section, with and without TMDs under pedestrian excitation.

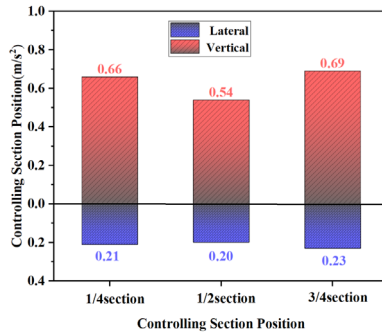


Fig. 11. Maximum acceleration response of each section based on Scheme III.

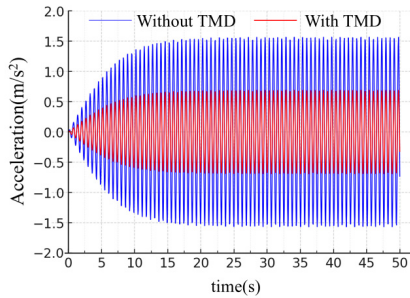


Fig. 12. Comparison of vertical acceleration of Scheme III.

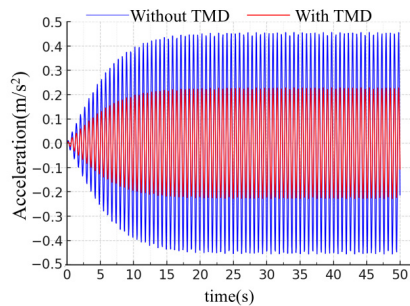


Fig. 13. Comparison of lateral acceleration of scheme III.

Scheme IV: Six Type-D TMDs are adopted, with two symmetrically arranged about the midpoint of the 1/4-span cross-section, two about the midpoint of the 1/2-span cross-section, and two about the midpoint of the 3/4-span cross-section. The acceleration responses of the pedestrian suspension bridge under pedestrian loading in different directions are illustrated in Figure 14. Figures 15 and 16 compare the time-history curves of vertical and lateral acceleration responses at the 1/4-span cross-section, with and without TMDs under pedestrian excitation.

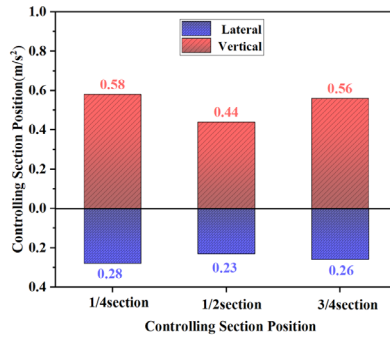


Fig. 14. Maximum acceleration response of each section based on Scheme IV.

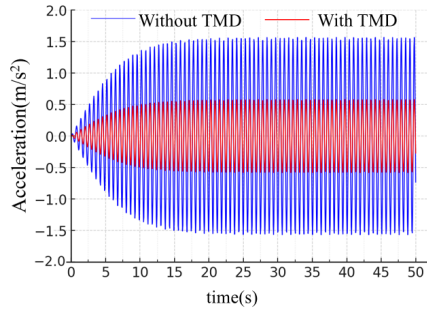


Fig. 15. Comparison of vertical acceleration of Scheme IV.

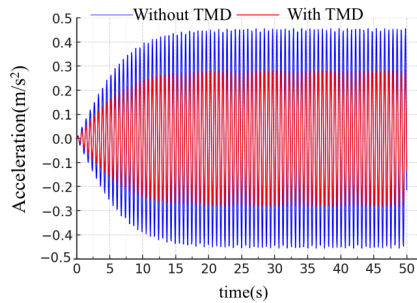


Fig. 16. Comparison of lateral acceleration of Scheme IV.

Figure 17 is plotted to illustrate the lateral and vertical vibration mitigation efficiency of each scheme, providing a clear and intuitive basis for analyzing the results and drawing conclusions.

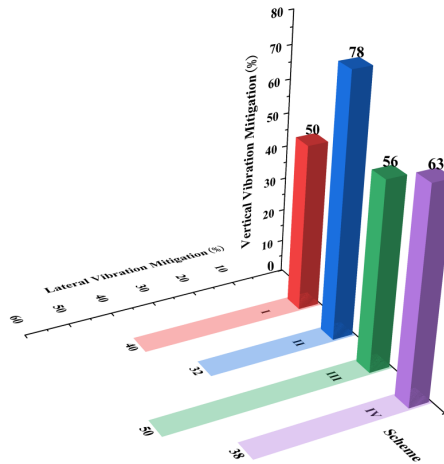


Fig. 17. Comparison of Vertical and Lateral Vibration Mitigation Efficiency under Different Schemes.

5 Conclusions

According to Tables 1 and 2, the use of an aluminum alloy deck system significantly improves the overall stiffness and fundamental frequency of the suspension bridge structure compared to the steel–wood composite deck. The change in deck mass leads to slight shifts in the modal frequencies of the two bridge models. Within the frequency range sensitive to pedestrian-induced vibrations, the corresponding mode shapes of the closely spaced modal frequencies in both bridges exhibit identical displacement characteristics.

According to Table 3, under the majority of analyzed loading conditions, the peak acceleration values at the observation points of both bridge models significantly exceed the CL2 comfort class (acceptable level). Moreover, the bridge equipped with the aluminum alloy deck exhibits slightly greater exceedance of the limit. Therefore, appropriate vibration mitigation measures are required in practical applications. The coupling effect between vertical and lateral vibrations induced by the inclined anti-wind cable system is negligible. As such, when analyzing the dynamic response data, it is sufficient to extract the acceleration response at a single observation point—corresponding to the peak modal displacement section—in the direction of the applied excitation.

A comparison of Figures 5 through 17 reveals that all TMD layout schemes demonstrate significantly higher vibration mitigation efficiency in the vertical direction than in the lateral direction. The vertical mitigation efficiency exceeds 50% across all schemes, reaching up to 78%, indicating that pedestrian loads predominantly excite

vertical modes and that TMDs tuned in the vertical direction can effectively absorb vibrational energy.

Among the specific schemes, Scheme II, which concentrates TMDs at key span locations (1/4, 1/2, and 3/4 spans), achieves the highest vertical mitigation efficiency, reaching approximately 75%. Scheme IV, while adopting the same span-wise TMD placement, arranges the devices symmetrically about the cross-sectional centerline, resulting in a more balanced distribution of lateral inertia and stiffness and thus improved lateral vibration mitigation compared to Scheme II. Scheme III, which also features symmetric cross-sectional placement but emphasizes the 1/4 and 3/4 spans, achieves the highest lateral mitigation efficiency at approximately 50%. These results suggest that concentrated placement at the cross-sectional center is more effective for vertical energy absorption, whereas symmetric placement about the cross-section enhances lateral energy dissipation.

Considering the overall vertical and lateral mitigation performance, constant total TMD mass, economic efficiency, and construction feasibility, Scheme II and Scheme IV are recommended. Scheme II offers optimal vertical vibration control and significantly enhances pedestrian comfort, while Scheme IV provides superior lateral mitigation performance without compromising vertical control, making it more suitable for projects with higher requirements for lateral comfort.

References

1. Xiao, X., Xue, H., and Chen, B., "Nonlinear Model for the Dynamic Analysis of a Time-Dependent Vehicle-Cableway Bridge System," *Applied Mathematical Modelling* 90:1049-1068, 2021.
2. Xie, H., Zhang, Y., and Cao, X., "A Method of Calculating Cable Change Parameters for Cableway Bridges," *Structures* 56:104965, 2023, doi:10.1016/j.istruc.2023.104965.
3. Tao, X., and Sun, J., "Design of Scenic-Area Pedestrian Cableway Bridges," *Highway Transportation Technology* 38(2):104-109, 2022 (in Chinese).
4. Yang, Y., Le, X., Zeng, J., et al., "Human-Induced Vibration Study of Guangzhou Haixin Bridge," *World Bridges* 51(4):70-76, 2023 (in Chinese).
5. Li, J., Ma, X., Wei, R., et al., "Comfort Analysis and Vibration-Reduction Design for a Large-Span Glass Suspension Footbridge," *World Bridges* 52(5):104-109, 2024 (in Chinese).
6. Wei, X. J., Zhang, J. W., Živanović, S., et al., "Dynamic Properties of Impact Hammer Operator and Their Influence on Dynamics of Lightweight Structures," *Journal of Sound and Vibration* 529:116932, 2022, doi:10.1016/j.jsv.2022.116932.
7. Xia, C., Wang, B., Luo, T., et al., "Dynamic Amplification Factor of Multi-Span Simply Supported Beam Bridge under Traffic Flow," *Advances in Structural Engineering* 25(8):1829-1847, 2022.
8. Sun, Y., "The Use of Aluminum Alloys in Structures: Review and Outlook," *Structures* 57:105290, 2023, doi:10.1016/j.istruc.2023.105290.
9. You, X., Xing, Z., Jiang, S., et al., "A Review of Research on Aluminum-Alloy Materials in Structural Engineering," *Developments in the Built Environment* 17:100319, 2024.
10. Mazzolani, F. M., "Competing Issues for Aluminium Alloys in Structural Engineering," *Progress in Structural Engineering and Materials* 6(4):185-196, 2004.

11. Qiao, Y., and Wu, G., "Human-Induced Vibration Research and Control for Single-Main-Cable Suspension Bridges," *World Bridges* 46(2):68-73, 2018 (in Chinese).
12. Li, Y., Yin, D. S., Wang, J. H., et al., "Framework for Calculating the Vertical Human-Induced Vibration of Suspension Footbridges under Random Pedestrian Flow," *International Journal of Steel Structures* 22(5):1322-1340, 2022, doi:10.1007/s13296-022-00640-z.
13. Xiang, Y., Chen, F., and Liu, R., "Comfort Evaluation of Pedestrian Suspension Bridges Based on Finite-Element Models," *Jiangxi Building Materials* 2024(5):95-100, 2024 (in Chinese).
14. Tang, J., and Yang, J., "Comfort Assessment of Human-Induced Vibration on Pedestrian Bridges," *Construction Technology (Chinese & English)*, e-pub ahead of print, 2025-03-22 (in Chinese).
15. Zhou, M., Wang, L., Xue, Z., et al., "Design and Vibration Characteristics of a Large-Span Curved Composite Pedestrian Bridge," *Industrial Construction*, 2022 (in Chinese).

Definitions

α_{opt}	The optimal frequency ratio between the TMD and the structural natural mode
ξ_{opt}	The optimal damping ratio of the TMD
k_{opt}	The optimal stiffness of the TMD
c_{opt}	The optimal damping coefficient of the TMD

Open Access This chapter is licensed under the terms of the Creative Commons Attribution-NonCommercial 4.0 International License (<http://creativecommons.org/licenses/by-nc/4.0/>), which permits any noncommercial use, sharing, adaptation, distribution and reproduction in any medium or format, as long as you give appropriate credit to the original author(s) and the source, provide a link to the Creative Commons license and indicate if changes were made.

The images or other third party material in this chapter are included in the chapter's Creative Commons license, unless indicated otherwise in a credit line to the material. If material is not included in the chapter's Creative Commons license and your intended use is not permitted by statutory regulation or exceeds the permitted use, you will need to obtain permission directly from the copyright holder.

